PERGAMON

Journal of Structural Geology 23 (2001) 619–638

JOURNAL OF STRUCTURAL GEOLOGY

www.elsevier.nl/locate/jstrugeo

# Displacement gradient and deformation in normal fault systems

David A. Ferrill[a,*], Alan P. Morris[b]

[a]*Center for Nuclear Waste Regulatory Analyses, Southwest Research Institute, 6220 Culebra Road, San Antonio, TX 78238, USA*
[b]*Division of Earth and Physical Sciences, The University of Texas at San Antonio, San Antonio, TX 78249, USA*

Received 20 December 1999; accepted 15 August 2000

**Abstract**

All fault systems contain faults with lateral (strike-parallel) displacement gradients. Lateral displacement gradients give rise to elongations parallel to fault cutoffs in either or both of the footwall and hanging wall fault blocks. We present a simple method for estimating cutoff parallel elongation based on geometric fault and fault-block elements. These elements are readily measured in the field or from maps and subsurface data, and include orientations of cutoff lines, faults, and displacement directions. Displacement gradients on overlapping normal faults produce relay ramps. Deformation within a relay ramp includes tilting, extension parallel to bounding cutoff lines, vertical axis rotation, and eventual breakthrough of the ramp. Relay ramp deformation is sensitive to fault displacement directions—oblique slip directions on the ramp bounding faults can cause contraction (restraining-step sense of displacement and overlap) or enhanced ramp extension (releasing-step sense of displacement and overlap). Relay ramp extension accommodated by brittle faulting and extension fracturing is important for locally altering porosity and permeability in fractured aquifers and reservoirs. Locally enhanced fault and extension fracture density can provide fast pathways for infiltration, percolation, and flow of groundwater, or barriers to fluid movement and can influence rock quality and stability of underground excavations. An example of strain localization in a displacement transfer zone from Yucca Mountain, Nevada, the proposed site for a high-level radioactive waste repository, is examined. 

## 1. Introduction

Displacement variation along faults is common and displacement gradients are typically steeper near fault terminations (tips) than on the fault as a whole (Dawers et al., 1993; Trudgill and Cartwright, 1994; Dawers and Anders, 1995). The presence of a displacement gradient requires that either one or both of the hanging wall and footwall cutoff lines must differ in length from their original, pre-faulting, lengths. The magnitude and partitioning of strain between footwall and hanging wall cutoffs depend on five factors:

1. dip of fault,
2. shape of fault (curved versus planar),
3. displacement gradient on fault,
4. degree of footwall uplift versus hanging wall subsidence, and
5. orientation of fault slip vector.

Relay ramps, which are common features of normal fault systems at all scales, are the products of opposite displacement gradients on two overlapping, laterally terminating, and subparallel normal faults (Fig. 1a; p. 533 in Ramsay and Huber, 1987; Larsen, 1988; Peacock and Sanderson, 1991, 1994; Trudgill and Cartwright, 1994; Childs et al., 1995; Huggins et al., 1995; Crider and Pollard, 1998). Relay ramps are bounded on one side by a hanging wall cutoff and on the other by a footwall cutoff. Because the bounding faults of a relay ramp have opposite displacement gradients (Fig. 1b, c), the ramp must experience deformation to maintain connectivity between hanging wall and footwall. This deformation is manifest as rotations about a vertical axis and one or more horizontal or low inclination axes (e.g., hinges at top and bottom of ramp) and as elongations parallel to cutoff lines, generated by the displacement gradients on the ramp-bounding faults (Fig. 1). In addition to relay-ramp-specific deformation, relay ramps may contain variable amounts of distributed deformation manifest, for example, by small faults parallel or synthetic to the bounding faults (e.g., Trudgill and Cartwright, 1994) or layer tilting in the fault dip direction (e.g., Huggins et al., 1995). This component of deformation compensates for the frequently observed cumulative displacement deficits at relay ramps seen in distance versus displacement profiles for segmented or overlapping faults (Trudgill and Cartwright, 1994; Huggins et al., 1995).

* Corresponding author.

0191-8141/01/$ - see front matter 
PII: S0191-8141(00)00139-5

In this paper we present a simple method for estimating cutoff-parallel elongation (extension or contraction) related to fault displacement gradient, that is applicable to deformation associated with the hanging wall and footwall of individual faults, or relay ramps between overlapping faults. The method is based on readily measured parameters such as the orientation of hanging wall and footwall cutoffs, fault dip, and fault displacement direction. Relay ramps in extensional fault systems are recognized as zones of localized high strain (e.g., Trudgill and Cartwright, 1994), related to the large displacement gradients on the bounding faults. This strain can be manifest in a variety of ways depending on the conditions of deformation. Relay ramps formed at shallow crustal levels are likely to exhibit high fracture densities (both faulting and jointing) which will influence fracture permeability. To illustrate applications of the technique, we consider natural examples of normal faulting from Yucca Mountain, Nevada, the proposed site for a high-level radioactive waste repository. Recent mapping of fault systems at Yucca Mountain has revealed the presence of several large breached relay ramps and indications that several smaller or more subtle relay structures may also be present. Fault system architecture and displacement gradients on Yucca Mountain faults are generally consistent with patterns of deformation predicted by our geometric model. These results indicate that some localized faulting is controlled by fault displacement gradients and interaction, rather than simply the regional stress field.

## 2. Conceptual framework

Relay ramps in brittle rocks transfer displacement between overlapping normal faults by vertical axis rotation (accommodating horizontal heave gradients on faults) and tilting (accommodating vertical throw gradients on the faults). A simple relay ramp can be simulated by making two parallel, overlapping cuts in a piece of paper, then extending the paper perpendicular to the cuts (e.g., see Fig. 1a). In the simple case where the paper is extended perpendicular to the fault traces without tearing, fold hinges localize at the fault (cut) tips at the top and bottom of the relay ramp, and fault displacement follows a circular arc, initially vertical, and eventually horizontal. The ramp is hinged at the top and bottom, and to avoid tearing, the paper is not extended within the ramp.

Rock is widely recognized as being weak in extension under brittle deformation conditions. Unlike the paper relay ramp described above, extension localized in a rock relay ramp is likely to produce permanent deformation. In the case of true dip slip on two overlapping, ramp-bounding normal faults, the ramp is geometrically required to: (i) rotate around a vertical axis, (ii) tilt, and (iii) extend parallel to hanging wall and footwall cutoff lines. The magnitude of this cutoff-parallel extension is directly related to the displacement gradients on the ramp-bounding normal faults (Figs. 1 and 2). In the case of an initially horizontal surface (represented only by footwall cutoff, FB and hanging wall cutoff, HB) cut by a terminating and planar normal fault (see triangle FBH in Fig. 2) with true dip-slip, both the footwall and hanging wall cutoff lines (see FB and HB, respectively, in Fig. 2) may experience extension.

Layer extension relates directly to the deflection of the hanging wall and/or footwall cutoff from the original horizontal position. Deflection of the cutoff lines is a function of fault displacement gradient. The anticipated cutoff-parallel extension in a relay ramp has both hanging wall and footwall cutoff components and can be estimated from a knowledge of: (i) the orientation of the ramp-bounding faults; (ii) the slip vector(s); and (iii) the orientations of the cutoff lines. This simplifies to knowing, for each bounding fault, the fault orientation, rakes of the hanging wall and footwall cutoffs within the respective faults, and the rakes of the slip vectors within the faults.

## 3. Geometric analysis

In this section, we provide a derivation of equations that allow estimation of cutoff-parallel elongation (positive = extension; negative = contraction) based on orientations of the fault, fault cutoff lines, and fault-slip vector. These equations apply to hanging wall or footwall deformation associated with any normal or normal-oblique slip fault with a lateral displacement gradient. For simplicity, we assume that prior to slip on the fault, the hanging wall and footwall cutoff lines were coincident and horizontal and that the fault dip and slip direction do not change during progressive deformation. However, the geometrical relationships and the model can be applied to a fault of any orientation if the position and orientation of the pre-faulting cutoff line is known or can be assumed.

Footwall cutoff-parallel elongation (Appendix A) is described by

$$e_{FW} = \frac{\sin(R_V)}{\sin(R_V - R_F)} - 1 \tag{1}$$

and hanging wall cutoff-parallel elongation by

$$e_{HW} = \frac{\sin(R_V)}{\sin(R_V + R_H)} - 1 \tag{2}$$

where $R_V$ is the rake of the fault's slip vector, $R_F$ is the rake of the footwall trace in the fault plane, and $R_H$ is the rake of the hanging wall trace in the fault plane (Fig. 2d and Appendix A).

Eqs. (1) and (2) are complementary and their solutions can substitute for each other by appropriate choice of angle convention. Using these relationships, strain can be estimated from the fault-dip ($\alpha$) and the rakes of the footwall ($R_F$) and hanging wall ($R_H$) cutoffs in the fault plane. Fig. 3 can be used to determine the cutoff-parallel elongation from the values of $R_F$ and $R_H$. In the simple case of pure dip-slip

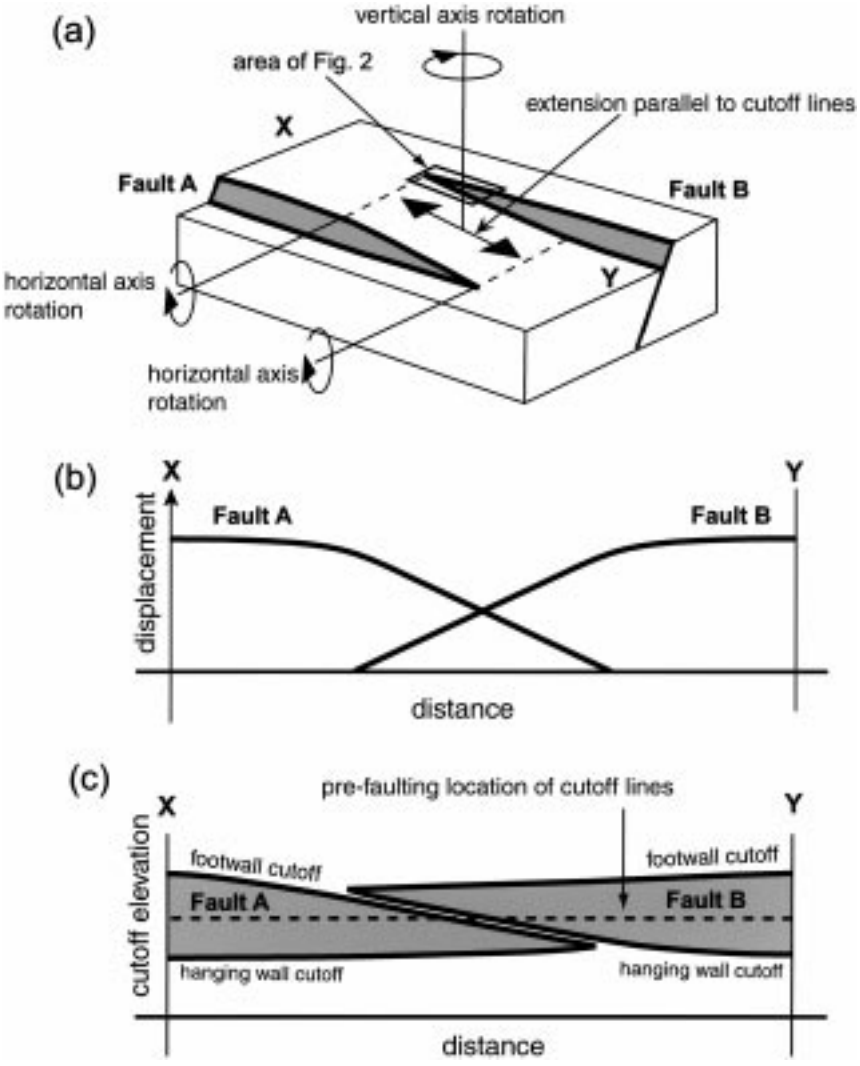


Fig. 1. (a) Schematic block diagram illustrating an extensional relay ramp. (b) Distance versus displacement diagram for the profile XY in (a). (c) Distance versus fault-cutoff elevation for the profile XY in (a).

($R_V = 90°$), all cutoff-parallel elongations are positive (i.e., length increase, Fig. 3). However, oblique slip can lead to zero or negative (shortening) cutoff-parallel strains.

In the case of the faults illustrated in Fig. 1a, a right-lateral slip component will cause the ramp-bounding cutoff lines to experience less extension than in the simple dip-slip case, and it may experience contraction in cases of a major strike-slip component. Conversely, a left-lateral strike-slip component would cause greater cutoff-parallel extension than the simple dip-slip case.

## 4. Cutoff-parallel elongation

### *4.1. Hanging wall versus footwall deflection*

Both footwall and hanging wall cutoffs of a normal fault can be deflected away from their pre-faulting position. Excellent field examples of deflections of both footwall and hanging wall cutoffs and various relay ramp geometries are exposed in the Volcanic Tableland north of Bishop, California (Fig. 4). Here a welded unit of the 738 ± 3 ka Bishop Tuff (Izett et al., 1988) is cut by several hundred faults ranging in displacement from less than 1 m to more than 100 m (Bateman, 1965; Dawers et al., 1993; Dawers and Anders, 1995; Willemse et al., 1996; Willemse, 1997; Ferrill et al., 1999a). The arid climate, relative youth, and resistance to weathering of the tuff result in remarkably well exposed fault-line scarps that closely approximate the fault geometries (Fig. 4). Although fault block geometries are well expressed by the topography, direct displacement direction indicators such as slickenlines are generally absent. These examples, however, serve to illustrate that footwall and hanging wall deflections can occur in a full range of relative proportions from hanging wall only to footwall only, and seemingly any combination of footwall and hanging wall deflection.

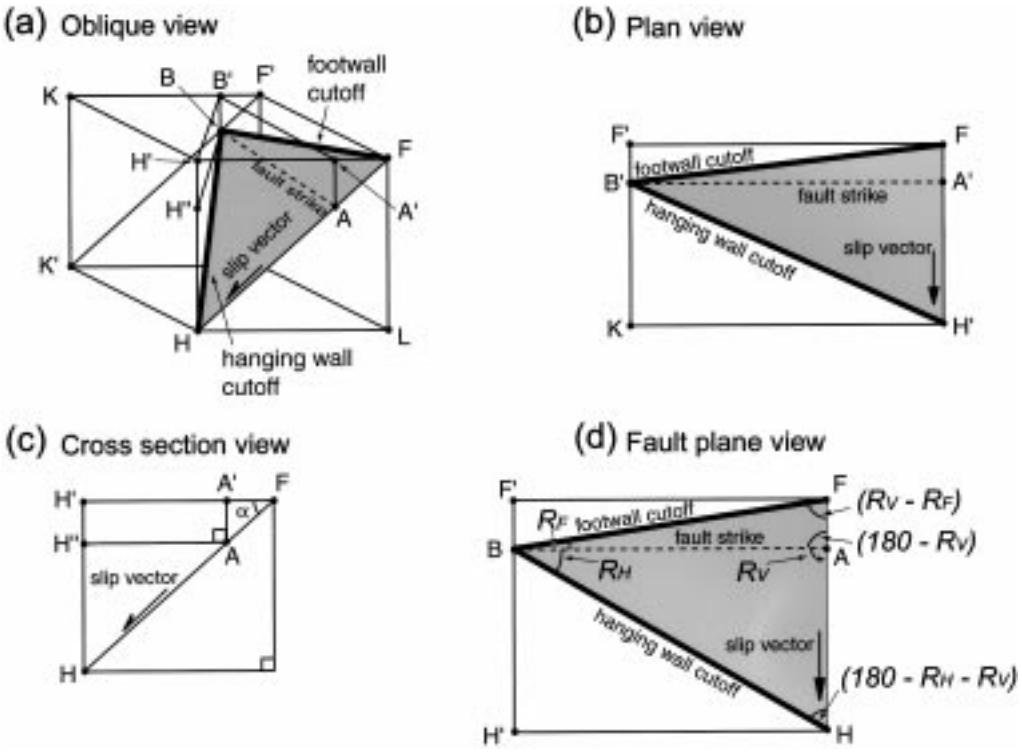


Fig. 2. (a) Cut-away block diagram of a fault gap (shaded triangular area) near a fault tip (point B) illustrating the geometric elements used in the analysis presented here. Shaded area represents fault surface, point A lies within the fault surface at the same elevation as the fault tip point B, lines FB and HB are footwall and hanging wall cutoff lines respectively. (b) Plan view of fault termination region. (c) Cross section view. (d) Fault plane view. $R_F$ = acute angle (rake) of footwall cutoff, measured as shown and counted as negative in Fig. 3; $R_H$ = acute angle (rake) of hanging wall cutoff, measured as shown and counted as positive in Fig. 3; $R_V$ = rake of slip vector, measured as shown from the strike line facing the fault slip vector, may have values from 0° to 180° (see also Fig. 5d, e, and Fig. 6a).

### 4.2. Hanging wall versus footwall cutoff elongation

Fig. 5 illustrates six possible combinations of cutoff deflections and fault slip that lead to different patterns of strain partitioning between the hanging wall and footwall (also see Table 1). In each case illustrated in Fig. 5, the faults dip 70° and the lateral gradient in fault gap (scarp) height is approximately the same. Fault displacement and total displacement gradients (measured in fault plane, parallel to slip vectors between hanging wall and footwall cutoffs) are the same for Fig. 5a, b, and c. Fig. 5a and b differ only in whether the hanging wall or footwall deforms. In these two cases, the deflected cutoff lines extend more than 6%. In 5c, both the hanging wall and footwall deform, and resulting cutoff extensions are less than 2%; considerably less than strains in the end member (one block rigid) cases (Fig. 5a and b). Oblique displacement on a fault (Fig. 5d and e) may produce extension in one fault block and contraction of the opposing fault block. For the idealized relay ramp shown in Fig. 5f, deflection of the hanging wall and footwall cutoffs that bound the ramp produces cutoff extensions of less than 2%.

### 4.3. Effects of oblique slip

In the simple case of true dip-slip faulting, fault block extension is expected (Fig. 6a, and b) and partitioning of strain into the footwall versus the hanging wall depends on the deflection of the hanging wall and footwall. Oblique slip produces more or less extension than expected for dip slip and depends on fault dip and slip direction.

If a normal fault has oblique slip (i.e., the slip vector rake, $R_V$, of the fault is not 90°), then certain displacement gradient and slip vector configurations may produce strain reversals during slip accumulation. For example, the hanging wall of a fault that dips 60°, has a slip vector rake of 80°, and that laterally tips to the left (looking down the slip vector plunge; Fig. 6c) will experience shortening followed by extension (Fig. 6d). Shortening of the ramp occurs from the start of displacement until the cutoff line is perpendicular to the slip vector, and further displacement causes the hanging wall cutoff to extend.

### 4.4. Relay ramp deformation

In the case of a relay ramp, the internal deformation should reflect deflection of the hanging wall and footwall cutoffs that bound the ramp. Equal deflection of hanging wall and footwall cutoffs (Fig. 1) by dip-slip produces uniform elongation across the width of the ramp and dip of the ramp in the fault-strike direction. Unequal deflection

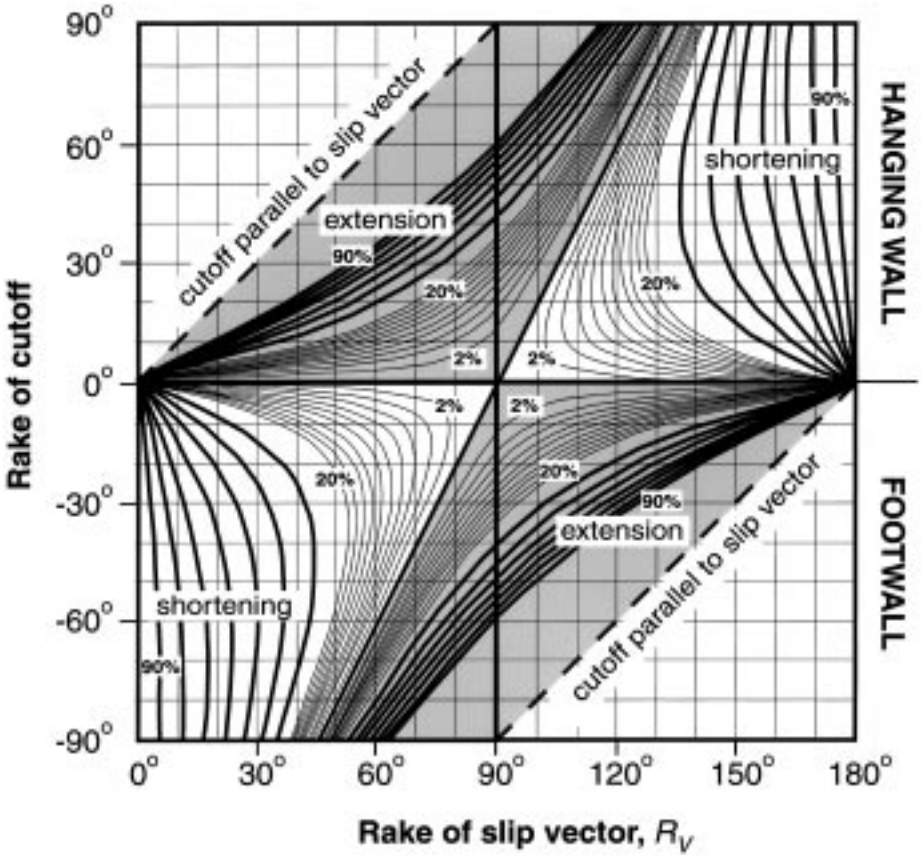


Fig. 3. Graphical solution to Eqs. (1) and (2) contoured with respect to percent elongation. Strain contours are in 10% increments (heavy solid lines) for values greater than 20%, and 2% increments (light solid lines) for values of 20% and less. Shaded areas represent extension ("positive" elongation), unshaded areas represent shortening ("negative" elongation). In order to estimate the elongation experienced by a cutoff line, first determine its rake in the fault plane. For example, if a hanging wall cutoff line has a rake of 30° in a pure dip-slip fault, its estimated elongation is 16% positive extension (rake of cutoff = +30°, rake of slip vector = 90°). A footwall cutoff with a rake of 30° on this same fault would experience the same extension (rake of cutoff = −30°, rake of slip vector = 90°).

of hanging wall and footwall cutoffs bounding a relay ramp would produce a deformation gradient across the ramp and is likely to produce tilting of the ramp toward the upthrown or downthrown side of the fault system.

The typical distance-displacement graph (e.g., Fig. 1b; Peacock and Sanderson, 1991; also see for example, fig. 5 in Dawers and Anders, 1995; Cartwright and Mansfield, 1998) gives no indication of this strain partitioning. A better representation is given by a graph of distance versus cutoff elevation (e.g., Fig. 1c; also see, for example, fig. 4b in Dawers and Anders, 1995, and fig. 6 in Huggins et al., 1995).

## 5. Progressive development of a relay ramp

The distribution and nature of deformation within a relay ramp depends not only on the five geometric components (fault-dip, fault shape, fault displacement gradients, orientation of slip vectors, and the degree of footwall uplift versus hanging wall subsidence of the bounding faults), but also on the temporal evolution of the ramp. Our geometric model (discussed in Section 3) accounts for fault-dip, displacement gradient, and slip vector, and because it is purely geometrical, can be applied to any segment of a cutoff line without *a priori* knowledge of faulting history. We discussed (in Section 4) the roles of the above factors on cutoff elongation and their possible effects on relay ramp strain. Here we consider the importance of the developmental history of the ramp in determining the overall strain present in a relay ramp.

As discussed earlier, relay ramps transfer displacement between two overlapping normal faults by tilting, vertical axis rotation, and cutoff-parallel elongation. In an ideal relay ramp, the relay ramp accomplishes all of the displacement transfer and lateral displacement-gradient related deformation, and rock outside the relay ramp is displaced but not tilted or internally deformed related to the lateral fault displacement gradients (see Fig. 5f for example). The Daisyhill relay ramp (fig. 6 in Huggins et al., 1995) is close to the ideal relay ramp geometry. The two bounding faults overlap but their displacement gradients are not

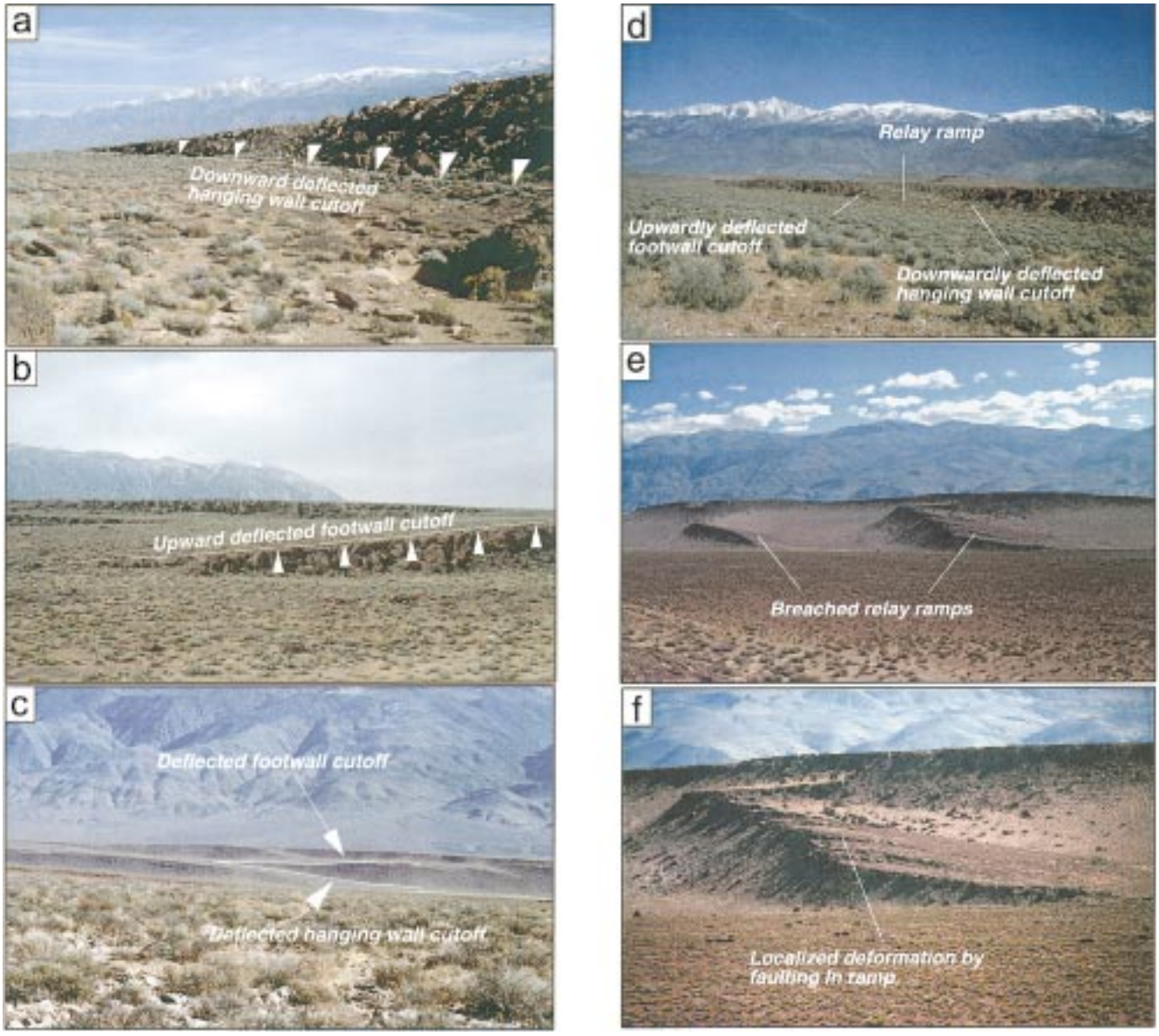


Fig. 4. Field photographs of unfaulted and breached relay ramps from the Volcanic Tableland, Owens Valley, California. Examples include: (a) fault gap defined by approximately horizontal footwall cutoff and deflected hanging wall cutoff; (b) fault gap defined by approximately horizontal hanging wall cutoff and deflected (upwardly bowed) footwall cutoff; (c) fault gap defined by deflected footwall and hanging wall cutoffs; (d) relay ramp bounded by deflected hanging wall and footwall cutoffs; (e) breached relay ramps bounded by deflected hanging wall and footwall cutoffs; and (f) detail of breached relay ramp illustrating small displacement faults (<5 m displacements) within breached ramp.

exactly complementary, thus the ramp dips obliquely basinward. Footwall cutoffs and hanging wall cutoffs of the two bounding faults have essentially the same elevations immediately adjacent to the ramp and the ramp has transferred all of the cumulative displacement imbalance between the two faults by means of its oblique dip (about 5°). Even in the ramp-bounding fault segments of the Daisyhill ramp, displacement gradients on the bounding faults are extremely low, on the order of 0.07. Predicted cutoff-parallel extension is commensurately low, about 0.4%, and this is consistent with the lack of mapped extension features in the ramp.

### 5.1. Alternative deformation paths

As is the case for many geologic structures, the final geometry of a structure is not necessarily indicative of a unique deformation path. In the case of a relay ramp, for example, the relay ramp has a geometry that is consistent with the displacement gradients on the two bounding faults. Faults may grow in a self-similar fashion (Fig. 7a), whereby the displacement to length ratio is consistent early in the development of the faults, and fault tip displacement gradients are constant throughout the faults' development until faults connect by relay ramp breaching. In this simple

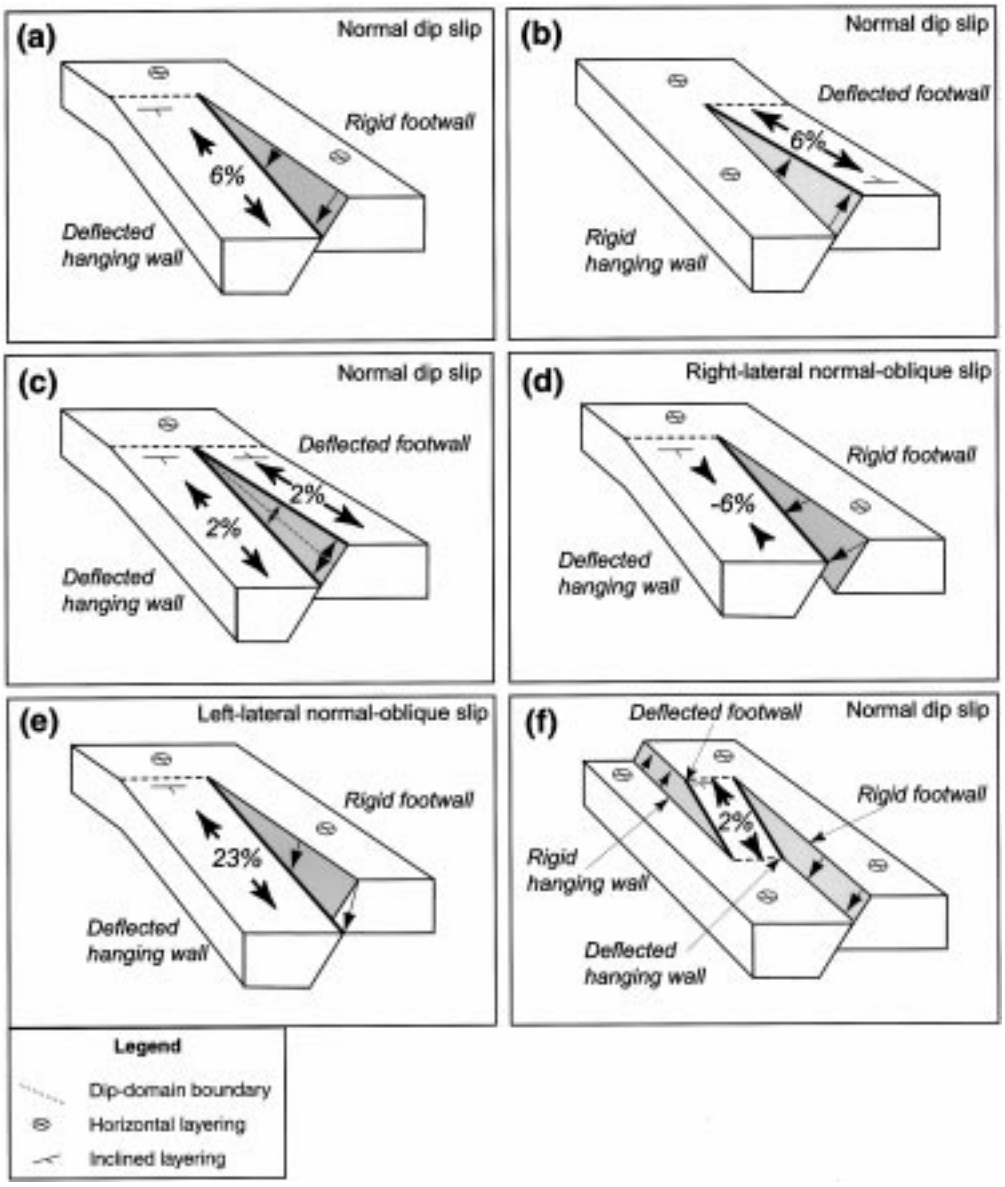


Fig. 5. Block diagrams illustrating different patterns of fault displacement and cutoff line deformation. Heavy lines are deformed cutoffs. Solid arrows in fault planes indicate displacement of hanging wall cutoff or footwall cutoff from initial position. (a) Rigid footwall, deforming hanging wall, dip-slip. (b) Deforming footwall, rigid hanging wall, dip-slip. (c) Deforming footwall, deforming hanging wall, dip-slip. (d) Rigid footwall, deforming hanging wall, contractional-oblique slip. (e) Rigid footwall, deforming hanging wall, extensional oblique-slip. (f) Ideal relay ramp bounded by fault tips with dip-slip.

Table 1
Geometric parameters and calculated elongations for fault displacement gradient examples illustrated in Fig. 4[a](numbers rounded to nearest whole number)

| Example[a] | | | Correlation to figures[b] | Measured angles (°) | | Fig. 3 cutoff rakes (°) | | Fig. 3 extension, % | |
|---|---|---|---|---|---|---|---|---|---|
| No. | FW | HW | | $\alpha$ | $R_v$ | $R_F$ | $R_H$ | $e_{FW}$ | $e_{HW}$ |
| 1 | Rigid | Def'd | Fig. 4a, Fig. 5a | 70 | 90 | 0 | 20 | 0 | 6 |
| 2 | Def'd | Rigid | Fig. 4b, Fig. 5b | 70 | 90 | − 20 | 0 | 6 | 0 |
| 3 | Def'd | Def'd | Fig. 4c, Fig. 5c | 70 | 90 | − 10 | 10 | 2 | 2 |
| 4 | Rigid | Def'd | Fig. 5d | 70 | 70 | 0 | 20 | 0 | − 6 |
| 5 | Rigid | Def'd | Fig. 5e | 70 | 110 | 0 | 20 | 0 | 23 |
| 6 | Def'd | Def'd | Fig. 4d, Fig. 5f | 70 | 90 | − 10 | 10 | 2 | 2 |

[a] Note that FW and HW refer to cutoffs on opposing sides of a single fault gap in examples 1–5, and cutoffs on opposing sides of a relay ramp in 6.
[b] Fig. 4 examples correlate in overall style (hanging wall versus footwall deflection) but not in detail (angles).

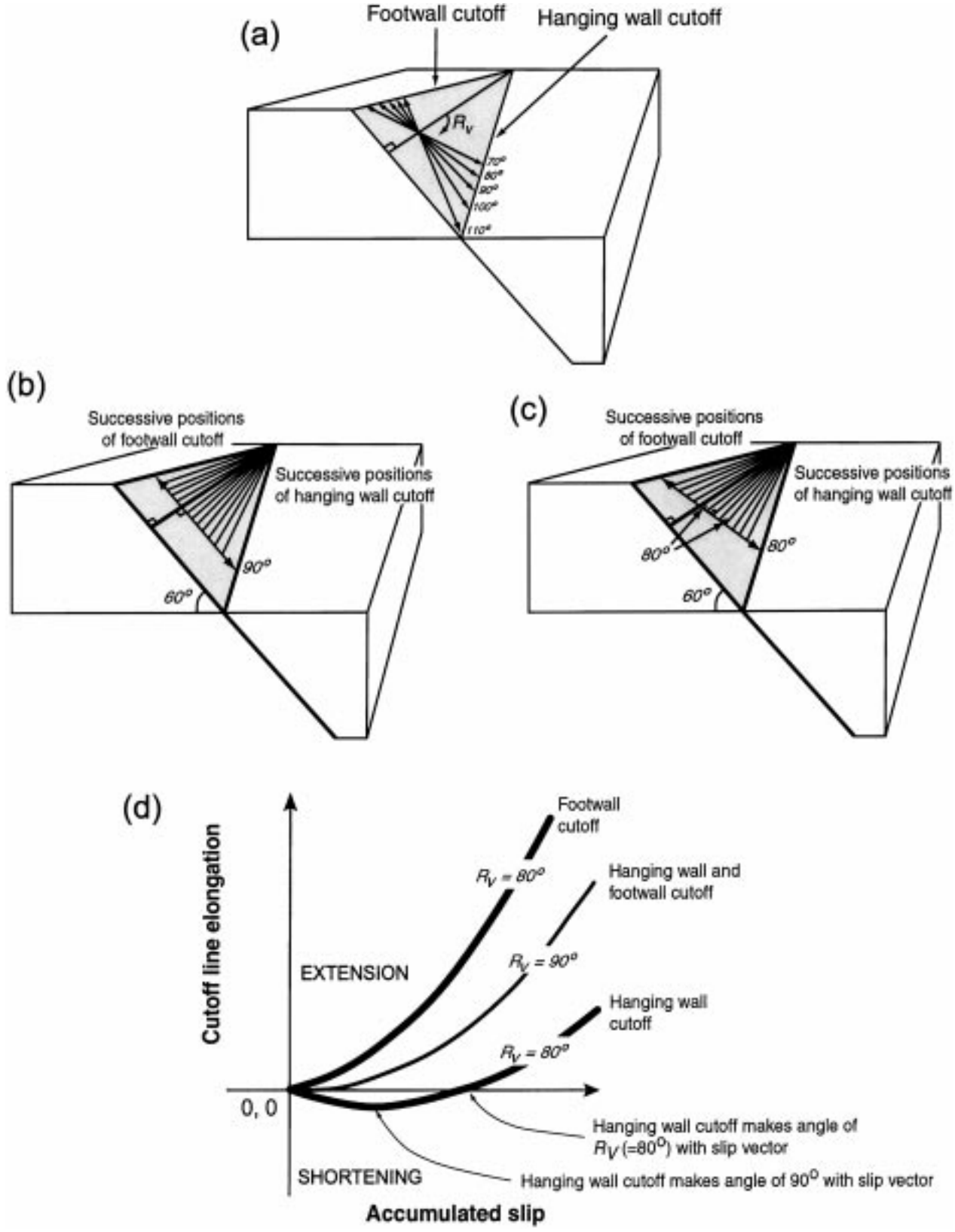


Fig. 6. (a) Block diagram illustrating the opposing influences of oblique slip on hanging wall and footwall cutoffs. (b) Block diagram illustrating displacement history of hanging wall and footwall cutoffs displaced along a dip-slip vector ($R_V = 90°$) (c) Block diagram illustrating displacement history of corresponding hanging wall and footwall cutoffs displaced along a slip vector with an 80° rake. (d) Graph of cutoff line elongation versus cumulative slip illustrates the progressive elongation of hanging wall and footwall cutoffs. Given the sense of oblique slip, the hanging wall cutoff undergoes shortening during early displacement until the cutoff line is perpendicular to the slip vector, and extension during subsequent displacement. In contrast, the footwall cutoff experiences extension throughout its deformation history.

conceptual model, the overlap to separation ratio will continue to increase until the relay ramp is breached. However, along an alternative deformation path, the bounding faults may propagate to their overlapping configuration rapidly, early in their development. Arrested propagation, but continued displacement, leads to increasing displacement to length ratio (Fig. 7b). In that case, the final overlap to separation ratio is produced early in the relay ramp development, then displacement produces increased tilting, vertical axis rotation, and internal deformation. A third possible case of relay ramp evolution may develop where fault tip propagation is arrested while the fault continues to accumulate displacement, which is then followed by a period of rapid fault tip propagation (Fig. 7c). In this third case, the displacement to length ratio will decrease with time. Fault propagation may proceed by one or a combination of the processes illustrated in Fig. 7b and c, which over time could produce the same geometry as self-similar propagation (Fig. 7a). However, depending on the magnitudes of fault-cutoff parallel elongation generated by displacement gradients at the propagating fault tips, permanent deformation by faulting may develop in the displacement transfer zone. Therefore, faults developed within a relay ramp or displacement transfer system during its progressive development may have orientations oblique or perpendicular to the bounding faults, depending on the evolutionary history. Deformation path depends on position on the controlling faults, shape and displacement patterns of fault planes, and other factors such as lithology and deformation conditions (e.g., Huggins et al. 1995).

### 5.2. Evolution of a conceptualized relay ramp

The displacement gradient along a fault generally increases toward its tips (fig. 2 in Dawers et al., 1993; fig. 11 in Scholz et al., 1993; fig. 4 in Trudgill and Cartwright, 1994; fig. 5 in Dawers and Anders, 1995; fig. 3 in Huggins et al., 1995; fig. 3 in Cartwright and Mansfield, 1998; fig. 2e in Ferrill et al., 1999a, b; fig. 5 in Moore and Schultz, 1999). Thus, two fault tips propagating past each other will generate a deformation front characterized by steep dips that will sweep through the relay zone. Depending on the history of the ideal relay ramp geometry (Figs. 4d, 5f, and 8a, b, c, and d), a dipping panel may develop that is initially oblique to the strike of the bounding faults (pre-overlap situation). The relay-ramp dip in the ideal case evolves to parallelism with the strike of the bounding faults (Fig. 8a and b) as fault overlap develops. The dip of this panel, and hence the extension it experiences, depends upon the displacement gradients and dips of the bounding faults. In cases where the bounding faults have steep displacement gradients near their tips, the obliquely dipping panel may experience sufficient extension to induce fracturing and faulting prior to full development of fault overlap (Fig. 8c). As overlap continues to develop, and the ramp extension direction rotates into parallelism with the strike of the bounding faults, the early formed faults will continue to be well oriented to accommodate extension by oblique slip, obviating the need for new faults to form and suppressing steeper dips in the ramp as a whole (Fig. 8d). Thus relay-ramp-breaching faults may be inherited from pre-overlap interaction between the principal bounding faults, and are likely to be oblique to the final ramp orientation.

In the ideal relay ramp, the "ultimate" footwall and hanging wall cutoffs (cutoff segments that do not immediately bound the relay ramp) attain essentially uniform elevations, and the relay ramp transfers all displacement between the faults. Such structures are common in nature and are well documented as examples of relay ramps (e.g., fig. 4 in Dawers and Anders, 1995; fig. 6 in Huggins et al., 1995), and fit the model described above (Sections 5.1 and 5.2). However, as illustrated in Section 4, the ultimate hanging wall and footwall cutoffs may also be deflected, which modifies the pattern of dipping panels associated with the propagating tips of the bounding faults (Fig. 8e and f).

## 6. Natural examples from Yucca Mountain, Nevada

### 6.1. Background

Yucca Mountain (Nevada, USA), the candidate site for the United States of America's first high-level radioactive waste repository, consists of a sequence of gently east-dipping Miocene volcanic tuff layers cut by a system of primarily west-dipping extensional faults. The distribution, characteristics, and future activity of faults and fractures at Yucca Mountain have several important implications for safety and long-term (10,000-year) performance of the candidate repository site, including: (i) controlling permeability architecture and groundwater flow rates and paths in the fractured tuff; (ii) influencing rock mass quality and tunnel stability; and (iii) providing sites for potential seismic activity and related fault block deformation (U.S. Department of Energy, 1998; U.S. Nuclear Regulatory Commission, 1999).

The Yucca Mountain fault system has been mapped in detail by Scott (1990), Simonds et al. (1995), and Day et al. (1998a,b). Extensional deformation has occurred in an evolving regional stress field, from E–W extension prior to 10 Ma, to WNW–ESE extension after 10 Ma (Zoback et al., 1981; Morris et al., 1996; Ferrill et al., 1999b). Day et al. (1998b) identified important relay structures at Yucca Mountain that consist of normal and oblique slip faults both within and cutting (breaching) relay ramps, curved fault tips bounding relay ramps, and right-lateral, strike-slip faults. Ferrill et al. (1999a) interpreted several of the bends in major faults to be corrugations introduced by fault linkage resulting from the breaching of former relay ramp structures (see Fig. 9a and b for relay structures at Yucca Mountain described in text).

In the context of the geometric models of fault block

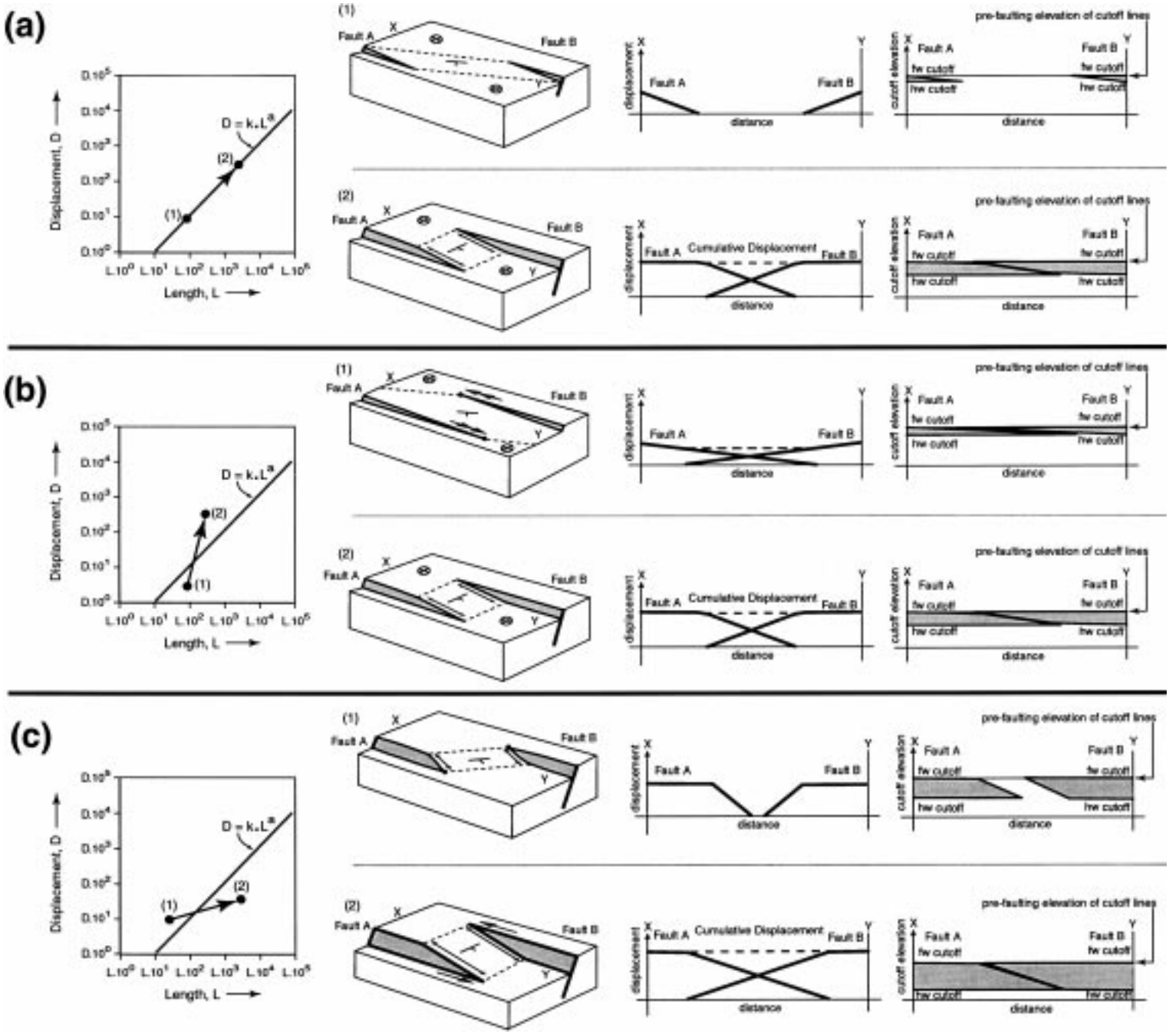
(a)
(b)
(c)
Displacement, D
Length, L
D = k.L^a
(1)
(2)
Fault A
Fault B
X
Y
Cumulative Displacement
distance
pre-faulting elevation of cutoff lines
cutoff elevation
fw cutoff
hw cutoff

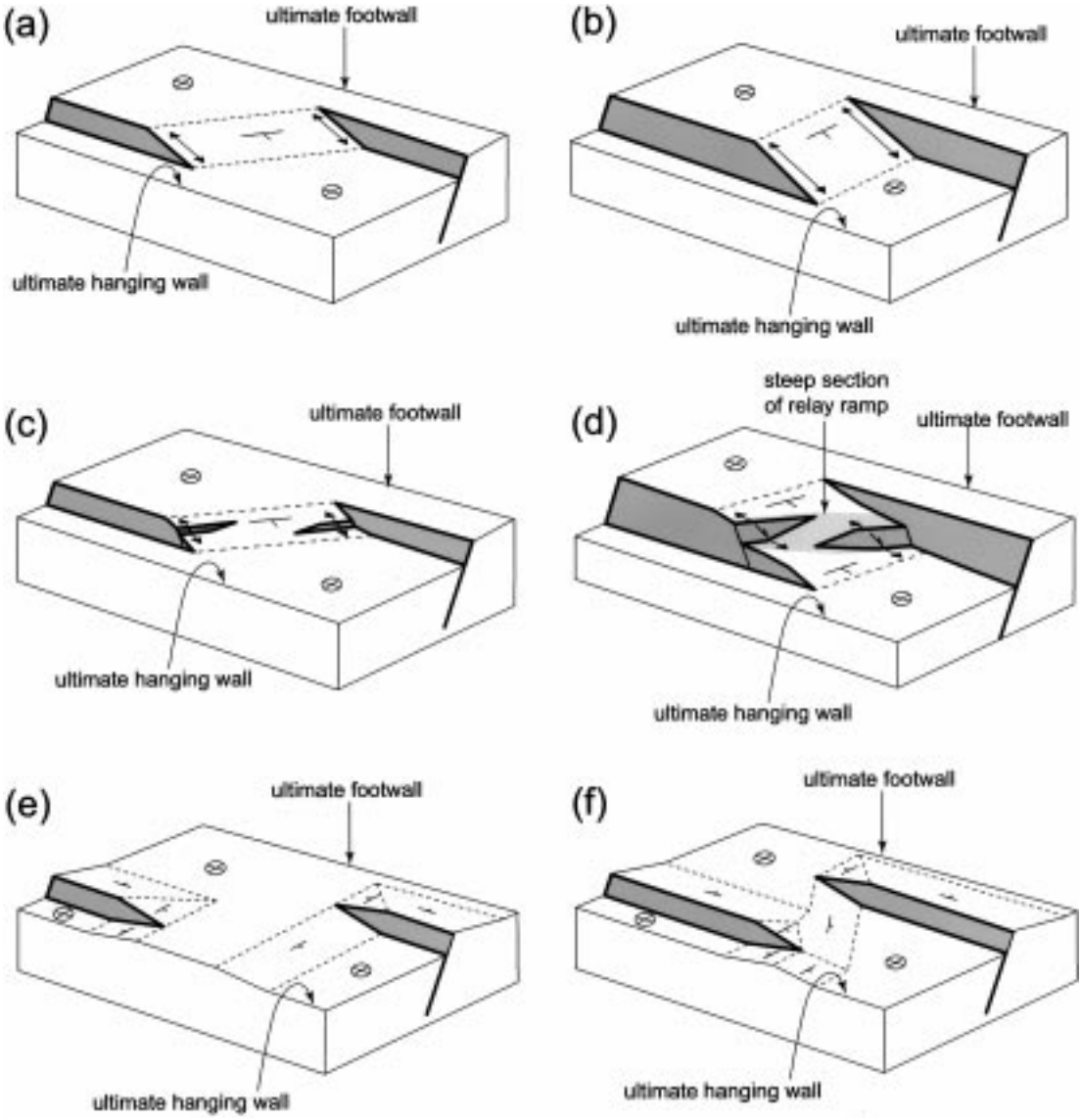


Fig. 8. Block diagrams illustrating the influence of relative footwall uplift and hanging wall subsidence on the evolution of deformation at underlapping and overlapping fault tips. (a) Pre-overlap situation with ideal relay ramp geometry. An oblique dip panel develops linking the tip regions of the bounding faults. (b) Overlap situation with ideal relay ramp geometry. The dipping panel evolves to geometry where the dip direction is parallel to the bounding fault cutoffs. (c) Pre-overlap situation with ideal relay ramp geometry and steep displacement gradients in the tip regions of the bounding faults. An oblique dip panel develops linking the tip regions of the bounding faults. In this case, however, the displacement gradients that produced oblique dip panel are sufficient to initiate formation of oblique faults within the relay ramp before the bounding faults have reached overlap. (d) Overlap situation with ideal relay ramp geometry and steep displacement gradients in the tip regions of the bounding faults. The bounding faults continue to propagate and extension directions within the ramp region rotate closer to parallelism with the bounding faults. This extension, however, can be accommodated by oblique slip on faults formed at an earlier stage in the ramp's evolution. This leads to the formation of an oblique steep section of the ramp which contains a high concentration of faults and is likely to become the locus of a ramp-breaching fault system. (e) Pre-overlap situation where the ultimate hanging wall and footwall deform by hanging wall subsidence and footwall uplift. (f) Overlap situation where the ultimate hanging wall and footwall deform by hanging wall subsidence and footwall uplift. See legend in Fig. 5 for explanation of symbols.

Fig. 7. Block diagrams illustrating influence of fault propagation and displacement gradient development on the formation of relay ramps. (a) Self-similar fault tip propagation, and no change in displacement gradients with time. (b) Rapid fault tip propagation and overlap development produces a low displacement gradient early in fault development. This stage is followed by arrested propagation and displacement accumulation, producing an increase in displacement gradient. (c) Arrested fault tip propagation produces a high displacement gradient which is followed by a period of rapid fault tip propagation and decrease in fault tip displacement gradient. See legend in Fig. 5 for explanation of symbols. The diagonal lines on graphs of displacement (D) versus length (L) represent the relationship between the two parameters, defined by constants $k$ and $a$ (see Dawers and Anders, 1995).

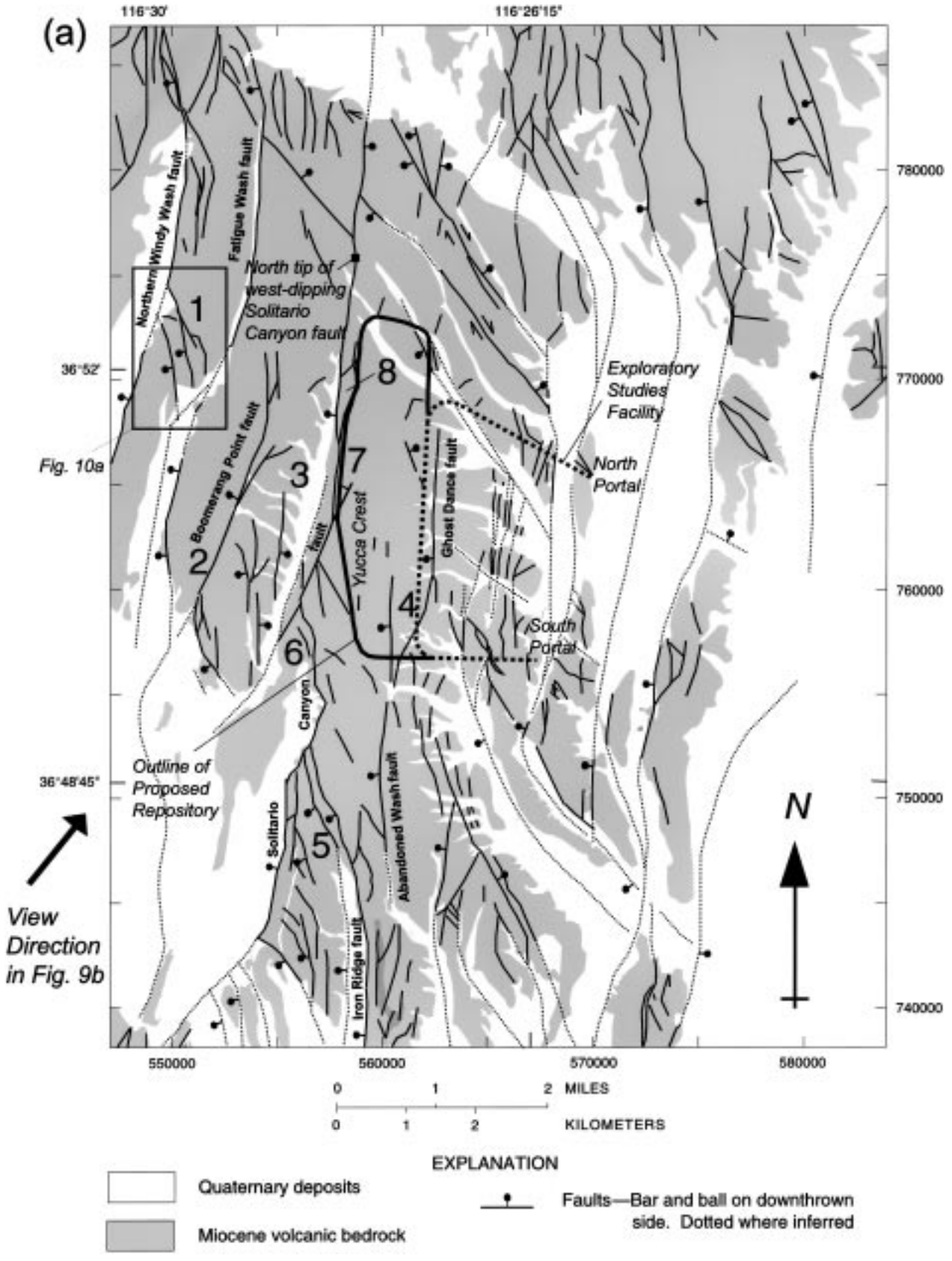


Fig. 9. (a) Map of Yucca Mountain faults after Day et al. (1998b). Annotations indicate positions of potential footwall, hanging wall, and relay ramp (combined hanging wall and footwall) deformation. (b) Oblique aerial photograph looking northeastward across western Yucca Mountain, Nevada. The Exploratory Studies Facility is a 7.8 km long, 7.6 m diameter tunnel through Yucca Mountain.

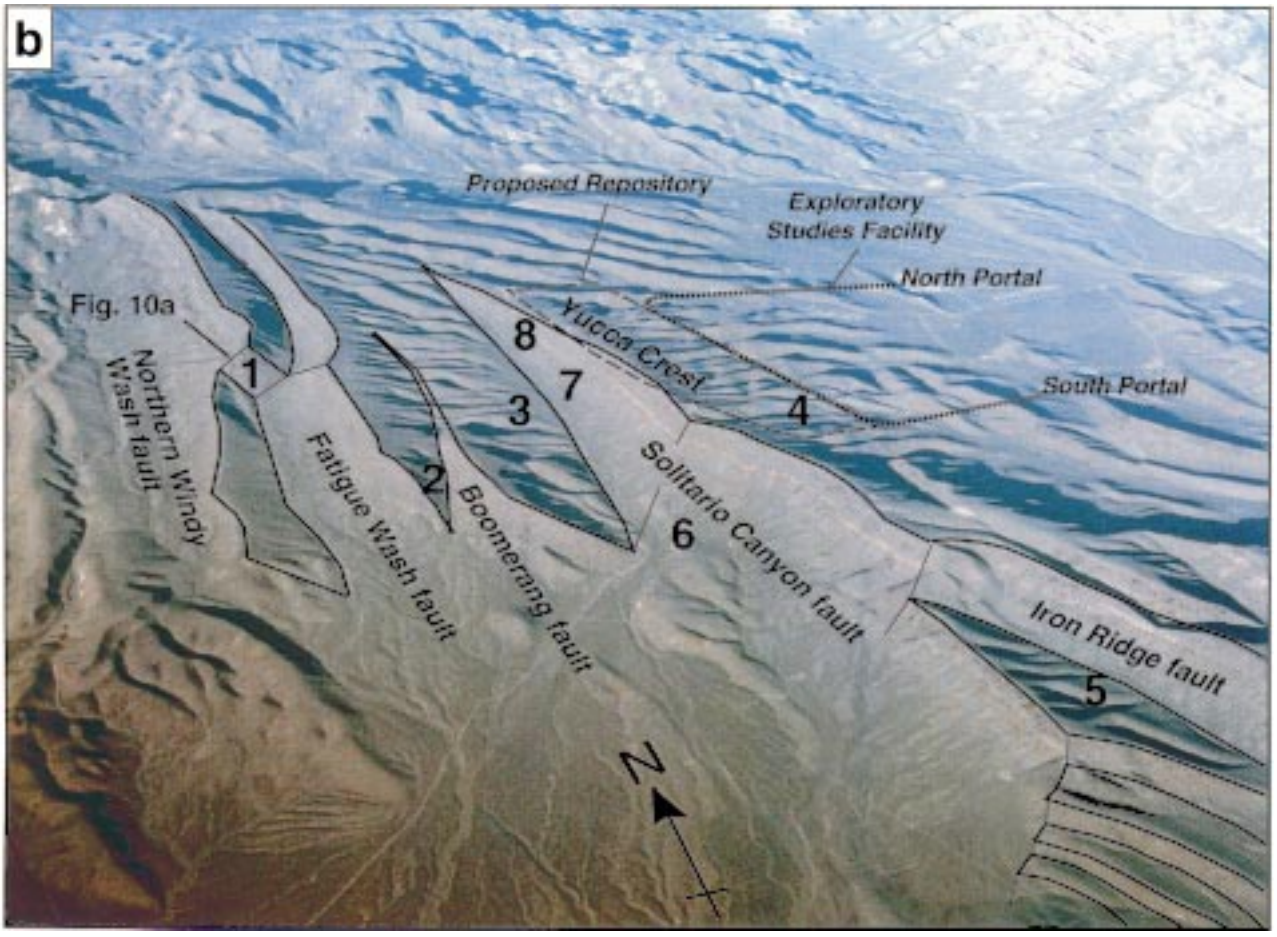


Fig. 9. (*continued*)

deformation presented in this paper, there are numerous geometric structural relationships at Yucca Mountain that may indicate hanging wall, footwall, or relay ramp deformation related to fault displacement gradients. One prominent case is the West Ridge connecting fault system that consists of several NW-trending extensional faults that connect the Northern Windy Wash and Fatigue Wash faults across West Ridge (see Fig. 9a and b, position 1). Note the pronounced deflection of the fault cutoffs that define the edges of West Ridge where the connecting fault system cuts the ridge (Fig. 9b).

Larger scale but more gentle fault-cutoff deflections are seen associated with the Boomerang Point and Solitario Canyon faults (positions 2 and 3, Fig. 9). Although the dominant deflection appears to be in the hanging wall of each of these faults, the footwall of the Solitario Canyon fault is bowed upward in the proposed repository location along Yucca Crest. This footwall bowing can be seen in a three-dimensional structural horizon display (see fig. 3a in Ferrill et al., 1999b). Also within the proposed repository location is an apparent displacement transfer zone (breached relay ramp) between the Ghost Dance and Abandoned Wash faults (position 4, Fig. 9).

We interpret at least four breached relay ramps along the Solitario Canyon fault (Fig. 9). The largest of these is the Solitario Canyon–Iron Ridge breached relay ramp (see position 5, Fig. 9). This ramp contains numerous NW-trending faults that, like the connecting fault system in West Ridge, are associated with pronounced deflection of the bounding cutoff lines (also see fig. 3 in Ferrill et al., 1999a). The next potential breached relay ramp to the north, based on mapped fault relationships and a pronounced footwall corrugation is at position 6 (Fig. 9a). We interpret that the breakthrough of this ramp occurred by curved lateral fault propagation along the footwall trace, leaving the breached relay ramp attached to the hanging wall block. Two more potential breached relay ramps along the Solitario Canyon fault are associated with the two NNE-trending splays of the Solitario Canyon fault that extend into the footwall of the main fault, and the northern tip of the Solitario Canyon fault (positions 7 and 8, Fig. 9a). The two NNE-trending splays of the Solitario Canyon fault may be relict tips of original fault segments that have since been connected by the formation of connecting fault systems. Relict relay ramp segments in the footwall in this case would have corresponding breached ramp segments in the hanging wall.

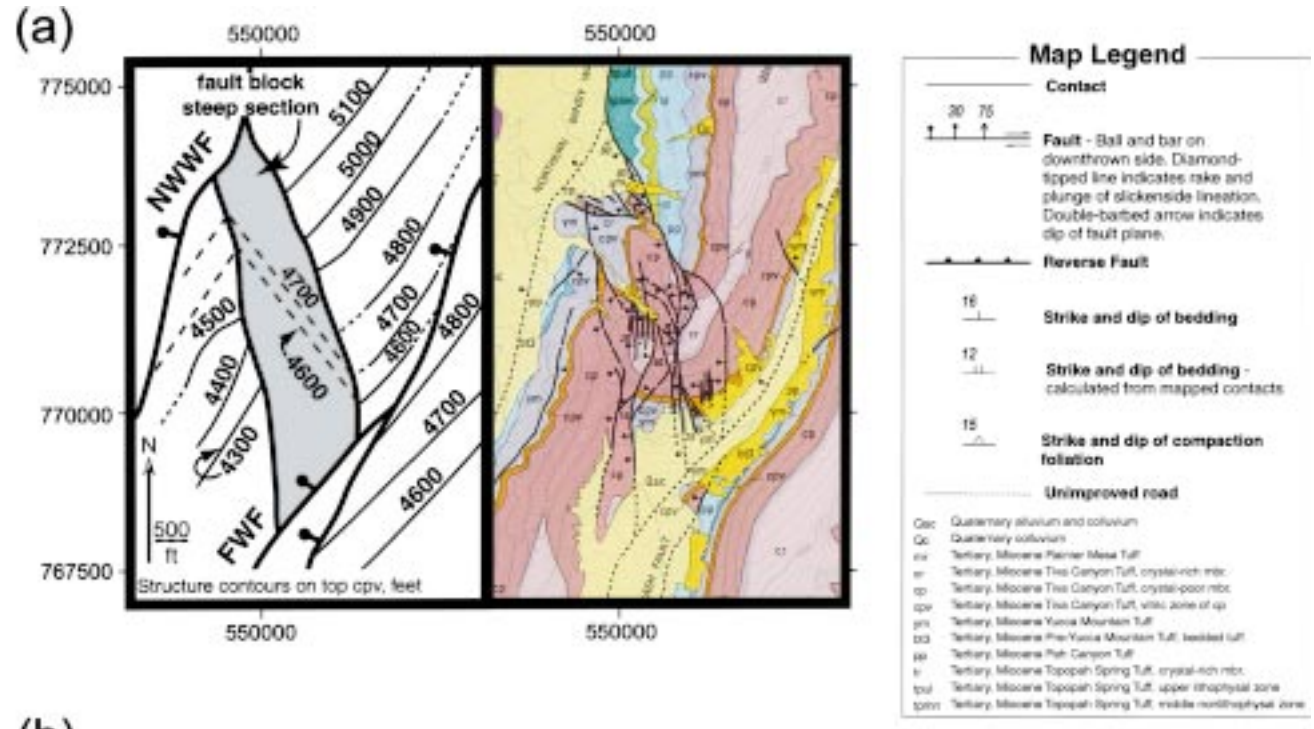
(a)
550000
550000
775000
772500
770000
767500
fault block
steep section
NWWF
FWF
5100
5000
4900
4800
4700
4600
4500
4400
4300
4700
4800
4600
4700
4600
N
500
ft
Structure contours on top cpv, feet
550000
550000
Map Legend
Contact
Fault - Ball and bar on downthrown side. Diamond-tipped line indicates rake and plunge of slickenside lineation. Double-barbed arrow indicates dip of fault plane.
Reverse Fault
Strike and dip of bedding
Strike and dip of bedding - calculated from mapped contacts
Strike and dip of compaction foliation
Unimproved road

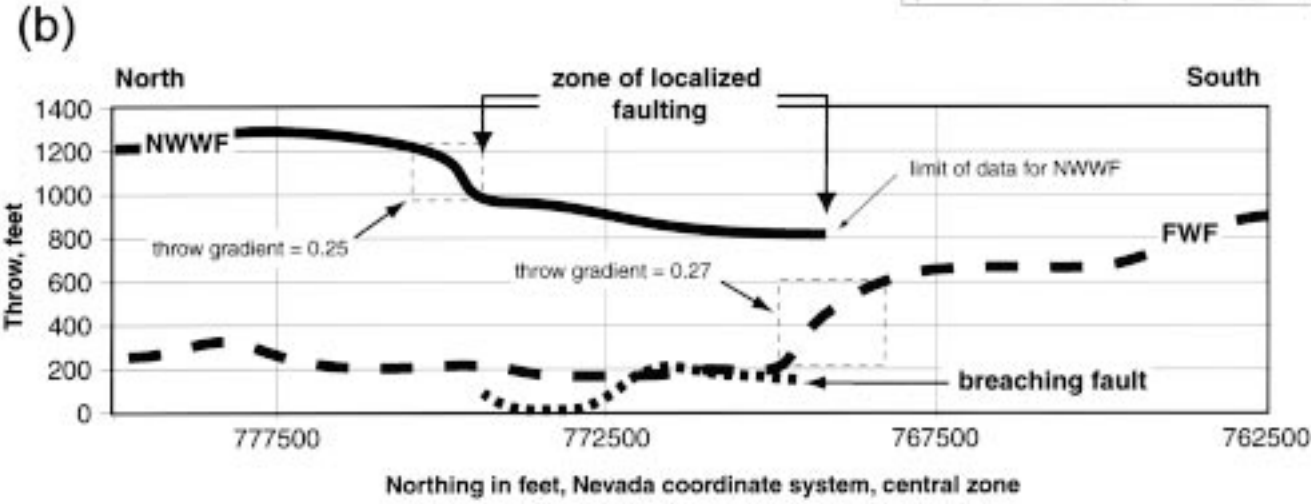
(b)
North
South
zone of localized faulting
NWWF
FWF
limit of data for NWWF
throw gradient = 0.25
throw gradient = 0.27
breaching fault
Throw, feet
1400
1200
1000
800
600
400
200
0
777500
772500
767500
762500
Northing in feet, Nevada coordinate system, central zone

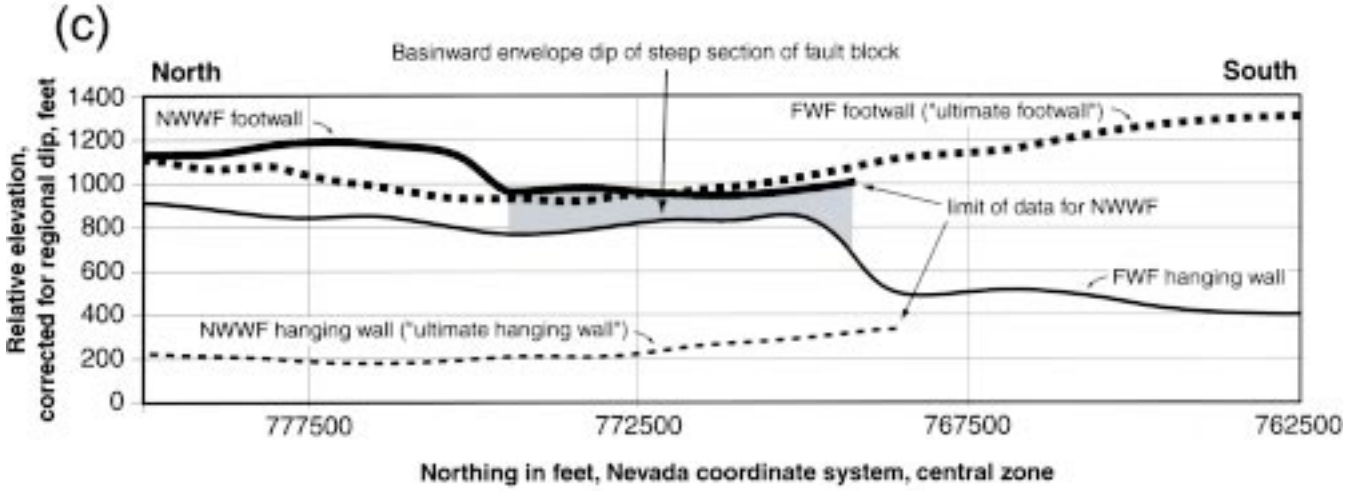
(c)
Basinward envelope dip of steep section of fault block
North
South
NWWF footwall
FWF footwall ("ultimate footwall")
limit of data for NWWF
FWF hanging wall
NWWF hanging wall ("ultimate hanging wall")
Relative elevation, corrected for regional dip, feet
1400
1200
1000
800
600
400
200
0
777500
772500
767500
762500
Northing in feet, Nevada coordinate system, central zone

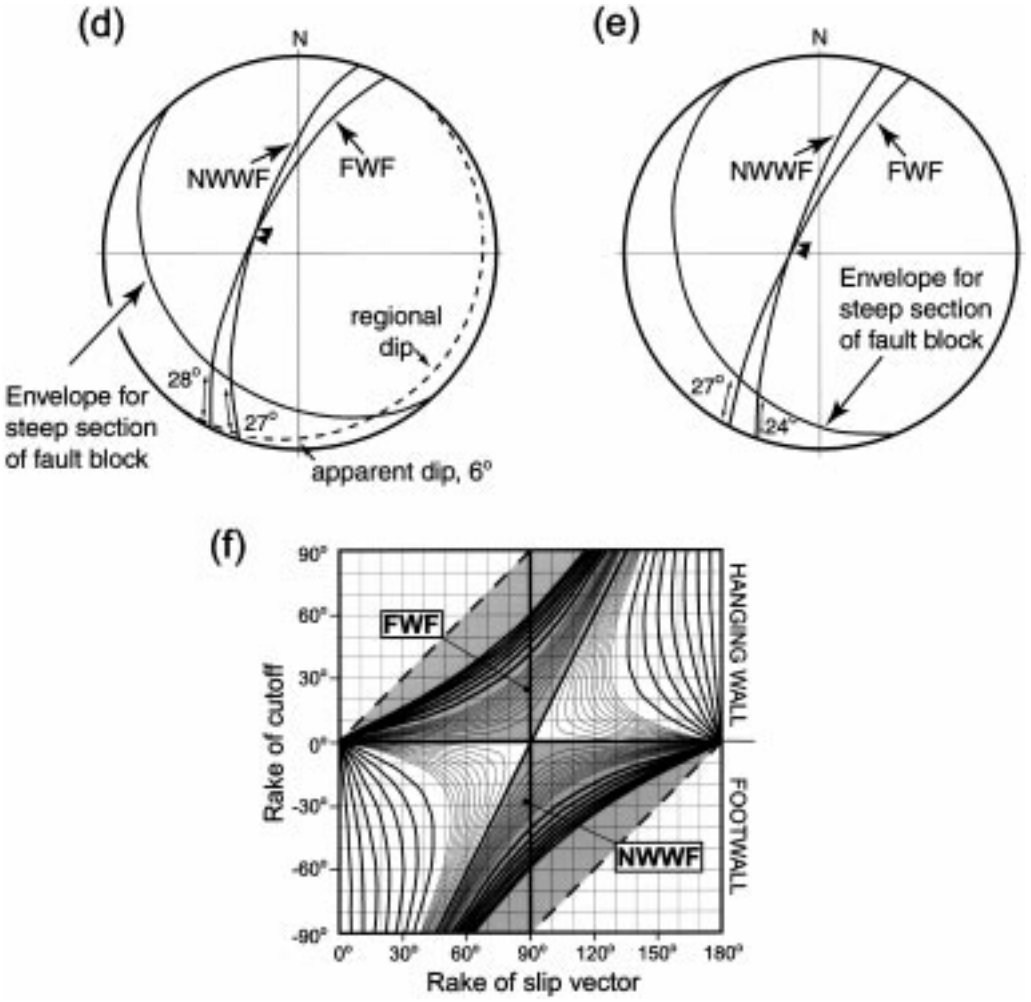


Fig. 10. (*continued*)

### *6.2. West Ridge connecting fault system, Yucca Mountain, Nevada*

Here we analyze the well-defined displacement transfer system between the Northern Windy Wash and Fatigue Wash faults (position 1, Fig. 9). The displacement transfer system is a narrow fault system (~500 m wide) that transfers displacement between two faults that overlap for a distance of about 10 km. Although not a classical relay ramp occupying the complete overlap between two fault tips, the displacement transfer system may have initiated during an earlier stage of development with less overlap. Using the geometrical model outlined in this paper, we estimate the strain in the ramp and compare it with observed structures. The map of Day et al. (1998b) is our primary data source (Fig. 10a). Structure contours are drawn for the top of the vitric zone of the crystal-poor member of the Tiva Canyon Tuff (cpv). All strikes and dips are given using

Fig. 10. The Northern Windy Wash fault (NWWF)–Fatigue Wash Fault (FWF) displacement transfer system. (a) Extract from the geologic map of Day et al. (1998b) (right) with the interpreted structure contours for the top of cpv (left). (b) Throw versus distance graph for the NWWF, FWF, and the breaching faults. Note the very high throw gradients on the bounding faults (NWWF and FWF) at the margins of the ramp steep section. These may partially represent "fossilized" fault tip throw gradients for these faults. These gradients generated the high strains within the oblique ramp steep section which in turn fixed the location of the ramp breaching fault(s). (c) Fault cutoff elevation versus distance graph for the NWWF and FWF. The north to south component of the regional dip has been removed by rotation. The ultimate footwall and hanging wall cutoffs follow the same trend through the graph, whereas the cutoffs that bound the steep section of the fault block show marked deflections. The mismatch in elevation between the ramp-bounding cutoffs reflects the oblique basinward dip of the steep section of the fault block (see also Huggins et al., 1995, fig. 6c). (d) Lower hemisphere, equal area projection of the geometric elements of the fault-block steep section in present-day coordinates. (e) Lower hemisphere, equal area projection of the geometric elements of the envelope of the steep section of the fault block, corrected for the regional dip. (f) Reference plot (see Fig. 3) to show how the bounding cutoffs of the ramp steep section can be used to determine cutoff-parallel elongation. **FWF**, Hanging wall cutoff against the FWF. The rake of the slip vector ($R_v$) is 89° and the rake of the cutoff = 24°. This yields an elongation of 10%. **NWWF**, Footwall cutoff against the NWWF. The rake of the slip vector ($R_v$) is 87°, and the rake of the cutoff = −27°. This yields an elongation of 10%.

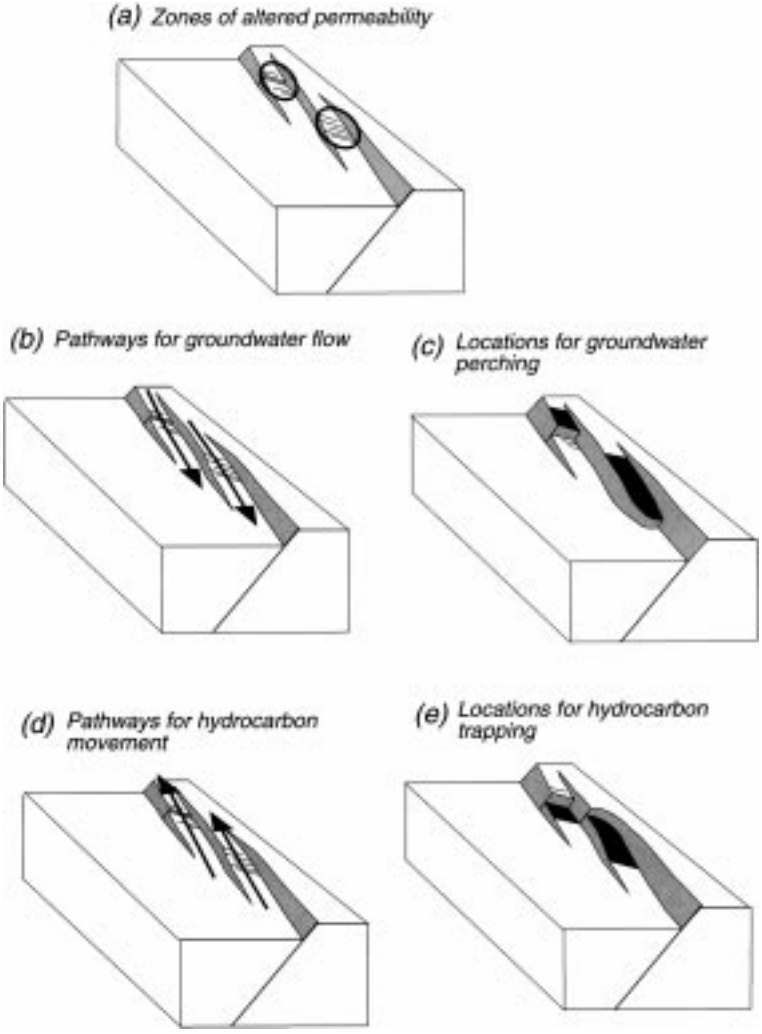


Fig. 11. Block diagrams illustrating aspects of fault interaction and fault block geometry and deformation important for groundwater flow and perching, and hydrocarbon migration and trapping. See figure 1 in Ferrill et al. (1999a) for progressive development of geometries illustrated in (c) and (e).

the right hand rule (reported dip is in direction 90° clockwise from reported strike azimuth), and we have used an average fault dip of 70° based on measurements of Day et al. (1998b). Fault throw versus distance, and cutoff elevation versus distance graphs (Fig. 10b and c) were drawn using data extracted from the U.S. Department of Energy's Geologic Framework Model (version 3.1; CRWMS M&O, 2000) combined with data from the Day et al. (1998b) map.

The Northern Windy Wash and Fatigue Wash faults have slightly different orientations (198/70 and 207/70 respectively). Structure contours reveal a NE–SW-trending, gently SE-dipping homocline (037/09) with a strike oblique to both faults (Fig. 10a). Between the two major faults is a rhomb-shaped panel trending approximately NNW–SSE that contains a system of relatively small, predominantly west dipping extensional faults. This system of faults has displaced the otherwise homoclinal fault block down to the southwest (Day et al., 1998b). The elevation of the top of the cpv NE of this panel is consistently 500 feet (152 m) higher than SW of the panel (along bounding fault strike). This panel is referred to here as the steep section of the fault block.

Both the Northern Windy Wash and Fatigue Wash faults exhibit extremely steep throw gradients (0.25 for the Northern Windy Wash fault and 0.27 for the Fatigue Wash fault) at the steep section of the fault block. In the cutoff elevation graph shown in Fig. 10c, the north-south component of the regional dip has been removed from the graph by rotating the graph 6° counterclockwise. Both bounding cutoff lines of the steep section of the fault block (Northern Windy Wash fault footwall and Fatigue Wash fault hanging wall) are strongly deflected, whereas the ultimate footwall and hanging wall show little deviation associated with the presence of the steep section of the fault block (Fig. 10c). This deflection pattern illustrates that all displacement transfer is accomplished in a narrow region, defined by the steep section of the fault block.

We interpret this displacement transfer system to have evolved similarly to the sequence schematically illustrated by Fig. 8c and d. The fault block steep section represents the

location at which elongations were sufficient to produce faulting, and may reflect the geometry of an obliquely dipping panel prior to overlap of the two bounding faults. The elevation change across the steep section, and its trend give an average envelope orientation for layering in the section of 140/27. Using a stereonet (Fig. 10d), the rake of the cutoff lines on the two bounding faults can be obtained: 28° in the Fatigue Wash fault and 27° in the Northern Windy Wash fault. Most of the slickenline measurements for the two bounding faults in the vicinity of this displacement transfer system indicate true dip-slip and therefore the rake of the slip vector is 90°. However, because the regional strike is oblique to the strikes of the bounding faults, and because our geometrical model depends on the angular difference between cutoffs in the fault plane, it is necessary to correct for the regional dip (Fig. 10e). The corrected values of the rakes of the envelope cutoff lines in the two bounding faults are: 24° in the Fatigue Wash fault and 27° in the Northern Windy Wash fault. The corrected values for the rakes of the slip vectors are: 89° in the Fatigue Wash fault and 87° in the Northern Windy Wash fault. The estimated extension of the envelope cutoffs both along the Fatigue Wash and the Northern Windy Wash faults are 10% (Fig. 10f). These extensions were sufficient to generate faulting in the displacement transfer zone.

### *6.3. Solitario Canyon fault footwall*

Cutoff-parallel elongations are not confined to relay structures and are to be expected wherever there is a displacement gradient along a fault. Finite, cutoff-parallel elongations may be small, but the propagation of a fault tip and its associated deformation front may generate incremental and progressive elongations that are sufficient to fracture rock. Although footwall uplift along the larger faults at Yucca Mountain is not extreme, it is nevertheless present, including along Yucca Crest (Fig. 9b). The footwall of the Solitario Canyon fault is bowed upward along Yucca Crest by 100 feet (30.5 m) along a strike distance of 3.7 miles (6 km) yielding an expected finite elongation of 0.006%. However, maximum footwall elevation gradients along the Solitario Canyon Fault are on the order of 0.07, yielding a local elongation of about 0.02%. During propagation of the fault, similar steeper throw gradients would have swept through the footwall adjacent to the fault and therefore they influence a large rock volume. The footwall of the Solitario Canyon fault includes the entire proposed repository volume.

Maximum throw gradients along the Solitario Canyon Fault are on the order of 0.24. The lack of major footwall deflection, associated with the large throw gradients, implies that much of the cutoff-parallel elongation that accompanied fault propagation was partitioned into the hanging wall of the fault. Therefore the rocks buried beneath alluvium in Solitario Canyon likely exhibit higher fracture (fault or joint) densities than the footwall. Similar analyses can be made for all the major faults in the Yucca Mountain area.

Analyses of extension associated with displacement gradients on the largest normal faults at Yucca Mountain may in time help to explain fracture orientations (e.g., east–west and NW–SE) that are not consistent with the evolution of the regional stress field (see for example Crider and Pollard, 1998). In addition to influencing the orientations of tectonic fractures at Yucca Mountain, we anticipate that relay ramps, and other deflected hanging wall and footwall blocks associated with lateral fault displacement gradients, are likely to be locations of enhanced fracture intensity. In the fractured welded tuff strata of Yucca Mountain, fracture intensity is a key factor that influences unsaturated and saturated zone water conductivity, locations of fast pathways for infiltration, percolation and flow, and rock quality and related tunnel stability.

## 7. Discussion

The method we describe for estimating ramp deformation from geometric elements is applicable to fault systems in different stages of evolution, from early stages where displacement gradients are small, relay ramps are gently dipping, and cutoff-parallel strains are small, to more mature fault systems where local displacement gradients are large, relay ramps have been breached by connecting faults, and associated extensional deformation in the ramp is evident (see fig. 1 in Ferrill et al., 1999a). Extensional relay ramps are ubiquitous and well documented features of normal fault systems. McFadzean et al. (1999) mentioned the common assumption of a correlation between overlap to separation ratio and hard-linking or breaching of relay ramps. However, they did not find a correlation between overlap to separation ratio and breakthrough. Our analysis shows that overlap to separation ratio is only one factor in the hard-linking of fault segments. Whether a relay ramp will be breached depends not only on its overlap and separation, but also on the cutoff-parallel strain it must accommodate. Breaching of a relay ramp depends primarily on the slip vectors and displacement gradients of its bounding faults.

Besides the local considerations of slip direction with respect to fault plane orientations, there is another potential control on fault block (including relay ramp) deformation—the overall displacement pattern on the entire system of normal faults. For an arcuate system of normal faults, dip slip on each fault will produce radial or convergent displacement patterns. In the case of radial displacement patterns, fault blocks may experience additional fault parallel extension, similar to the radial thrusting model described by Ferrill and Groshong (1993). Conversely, convergent displacement on an arcuate array of normal faults, such as the Grabens fault system in Canyonlands National Park, Utah (cf., McGill and Stromquist, 1979; Trudgill and

Cartwright, 1994) or fault-bounded minibasins in the Gulf of Mexico (cf., Diegel et al., 1995; Rowan et al., 1999), may produce a component of fault-strike-parallel fault block shortening. Such a pattern of convergent displacement may lead to reduced extension in relay ramps and may permit greater fault displacement prior to breaching of relay ramps.

The development and evolution of relay ramps have several important implications for fluid movement in normal fault systems (Fig. 11). Relay ramps and breached relay ramps are important pathways for hydrocarbon migration in normal fault systems (Morley et al., 1990; Peacock and Sanderson, 1994). Relay ramps provide unbroken reservoir connectivity through fault systems, and identification of their presence or likelihood is critical in trap risk assessment, and for planning efficient reservoir production strategies. Breached relay ramps, and footwall closures related to normal fault displacement gradients also provide important hydrocarbon traps in normal fault systems (Morley et al., 1990; Peacock and Sanderson, 1994). Similarly, relay ramps are important groundwater flow pathways in aquifers where aquifer strata are offset from other permeable strata across faults, or where fault zones are relatively impermeable (Collins and Hovorka, 1997; Hovorka et al., 1998). Breached relay ramps may result in perching or isolation of some portions of aquifer systems. Deformation related to normal fault displacement gradients, as is common in relay ramps, may be manifest by localized fault and joint development. Consequently, fault block sections associated with large lateral displacement gradients on bounding normal faults may have locally enhanced or reduced permeability, depending on the deformation mechanisms. This can be important for aquifer or reservoir productivity. As discussed above, simple, easily measured geometric parameters can be used to estimate the magnitude of this localized deformation.

## 8. Summary

All fault systems contain faults with lateral (along strike) displacement gradients. In this paper, we have developed a geometrical model for normal fault-block internal deformation related to fault displacement gradients that leads us to expect increasing fault cutoff-parallel extension with increasing normal fault displacement gradients. Oblique slip directions and convergent or divergent slip directions within a fault array may lead to reduced or enhanced local extension with respect to extension anticipated from an array of parallel dip-slip normal faults.

In the context of the geometric models of fault block deformation presented in this paper, we find that there are numerous structural relationships at Yucca Mountain, Nevada that indicate localized deformation (e.g., zones of intense fracturing) related to fault displacement gradients. Deformation related to lateral fault displacement gradients may help to explain fracture orientations at Yucca Mountain that are not consistent with the evolution of the regional stress field. This analysis provides a conceptual basis for assessing the fracture framework at Yucca Mountain; a key factor in the analysis of groundwater flow, tunnel stability, and possible future distributed deformation related to fault slip.

## Acknowledgements

This paper was prepared as the result of work performed at the Center for Nuclear Waste Regulatory Analyses (CNWRA). Some of the concepts and examples (Volcanic Tableland) described here were originated during development of the CNWRA structural geology field course for the oil and gas industry and were funded through internal (Southwest Research Institute) funding. Subsequent development of the concepts and analyses of Yucca Mountain faulting were conducted for the U.S. Nuclear Regulatory Commission (NRC) under contract number NRC-02-97-009. The paper is an independent product of the CNWRA and does not necessarily reflect the views and regulatory position of the NRC. We thank Annette Mandujano and Rebecca Emmot for assistance in manuscript preparation, Barbara Long for editorial review, and Darrell Sims and Deborah Waiting for assistance in figure preparation. We thank Jim Handschy, Darrell Sims, John Stamatakos, Bill Dunne, and Juliet Crider for valuable discussions of normal faulting and Darrell Sims, Wesley Patrick, and Budhi Sagar for technical reviews that greatly improved the original manuscript. Comments by NRC reviewers Philip Justus, Lee Abramson, and John Trapp, JSG reviewers Nancye Dawers and Joe Cartwright, and editorial work of Richard Lisle led to considerable improvement of the final manuscript.

## Appendix A. Cutoff-parallel elongation

The original length of each cutoff line would have been AB. The deformed lengths are FB, for the footwall and HB for the hanging wall. Cutoff-parallel elongations, $e$, for the footwall ($e_{FW}$) and hanging wall ($e_{HW}$), based on original and deformed cutoff lengths, are defined as follows:
footwall,

$$e_{FW} = \frac{FB}{AB} - 1$$

and hanging wall,

$$e_{HW} = \frac{HB}{AB} - 1.$$

Using the fault plane section (Fig. 2) and the law of sines, the footwall cutoff length is

$$\frac{FB}{\sin(180 - R_V)} = \frac{AB}{\sin(R_V - R_F)}$$

where: $R_V$ = Rake of slip vector in the fault; $R_F$ = Rake of footwall cutoff line in the fault. In terms of cutoff-parallel extension ($e$), the footwall cutoff extension is

$$\frac{FB}{AB} = \frac{\sin(180 - R_V)}{\sin(R_V - R_F)} = (1 + e_{FW})$$
$$e_{FW} = \frac{\sin(180 - R_V)}{\sin(R_V - R_F)} - 1 = \frac{\sin(R_V)}{\sin(R_V - R_F)} - 1 \quad \text{(A1)}$$

The hanging wall cutoff length is

$$\frac{HB}{\sin(R_V)} = \frac{AB}{\sin(180 - R_V - R_H)}$$

In terms of cutoff-parallel extension ($e$), the hanging wall cutoff extension is

$$\frac{HB}{AB} = \frac{\sin(R_V)}{\sin(180 - R_V - R_H)} = (1 + e_{HW})$$
$$e_{HW} = \frac{\sin(R_V)}{\sin(180 - R_V - R_H)} - 1 = \frac{\sin(R_V)}{\sin(R_V + R_H)} - 1 \quad \text{(A2)}$$

where $R_H$ = rake of hanging wall cutoff in the fault.

## References


Bateman, P.C., 1965. Geology and tungsten mineralization of the Bishop District, California. USA. Geological Survey Professional Paper 470.

Cartwright, J.A., Mansfield, C.S., 1998. Lateral displacement variation and lateral tip geometry of normal faults in the Canyonlands National Park, Utah. Journal of Structural Geology 20, 3–19.

Childs, C., Watterson, J., Walsh, J.J., 1995. Fault overlap zones within developing normal fault systems. Journal of the Geological Society. London 152, 535–549.

Collins, E.W., Hovorka, S.D., 1997. Structure map of the San Antonio segment of the Edwards Aquifer and Balcones fault zone, south-central Texas: Structural framework of a major limestone aquifer: Kinney, Uvalde, Medina, Bexar, Comal, and Hays Counties. The University of Texas at Austin, Bureau of Economic Geology Miscellaneous Investigations Map No. 38.

Crider, J.G., Pollard, D.D., 1998. Fault linkage: Three-dimensional mechanical interaction between echelon normal faults. Journal of Geophysical Research 103 (B10), 24373–24391.

CRWMS M&O, 2000. Geologic Framework Model (GFM3.1) Analysis Model Report. MDL-NBS-GS-000002 Rev 00 ICN 01. Las Vegas, Nevada: Civilian Radioactive Waste Management System Management & Operating Contractor. ACC: MOL. 20000121.0115.

Dawers, N.H., Anders, M.H., 1995. Displacement-length scaling and fault linkage. Journal of Structural Geology 17, 607–614.

Dawers, N.H., Anders, M.H., Scholz, C.H., 1993. Growth of normal faults: Displacement-length scaling. Geology 21, 1107–1110.

Day, W.C., Potter, C.J., Sweetkind, D., Dickerson, R.P., San Juan, C.A., 1998a. Bedrock geologic map of the Central Block area, Yucca Mountain, Nye County, Nevada. U.S. Geological Survey Miscellaneous Investigations Series Map I–2601, scale 1:6000.

Day, W.C., Dickerson, R.P., Potter, C.J., Sweetkind, D.S., San Juan, C.A., Drake, II, R.M., Fridrich, C.J., 1998b. Bedrock geologic map of the Yucca Mountain area, Nye County, Nevada. U.S. Geological Survey Miscellaneous Investigations Series Map I–2627, scale 1:24,000.

Diegel, F.A., Karlo, J.F., Schuster, D.C., Shoup, R.C., Tauvers, P.R., 1995. Cenozoic structural evolution and tectono-stratigraphic framework of the northern Gulf Coast continental margin. In: Jackson, M.P.A., Roberts, D.G., Snelson, S. (Eds.). Salt Tectonics: A Global Perspective. AAPG Memoir 65, pp. 109–151.

Ferrill, D.A., Groshong Jr., R.H., 1993. Kinematic model for the curvature of the northern Subalpine Chain, France. Journal of Structural Geology 15, 523–541.

Ferrill, D.A., Stamatakos, J.A., Sims, D., 1999a. Normal fault corrugation: Implications for growth and seismicity of active normal faults. Journal of Structural Geology 21, 1027–1038.

Ferrill, D.A., Winterle, J., Wittmeyer, G., Sims, D., Colton, S., Armstrong, A., Morris, A.P., 1999b. Stressed rock strains groundwater at Yucca Mountain, Nevada. GSA Today 9 (5), 1–8.

Hovorka, S.D., Mace, R.E., Collins, E.W., 1998. Permeability structure of the Edwards Aquifer, south Texas—Implications for aquifer management. The University of Texas, Bureau of Economic Geology, Report of Investigations No. 250.

Huggins, P., Watterson, J., Walsh, J.J., Childs, C., 1995. Relay zone geometry and displacement transfer between normal faults recorded in coal-mine plans. Journal of Structural Geology 17, 1741–1755.

Izett, G.A., Obradovich, J.D., Mehnert, H.H., 1988. The Bishop ash bed (middle Pleistocene) and some older (Pliocene and Pleistocene) chemically and mineralogically similar ash beds in California, Nevada, and Utah. United States Geological Survey Bulletin 1675.

Larsen, P.-H., 1988. Relay structures in a Lower Permian basement-involved extension system, East Greenland. Journal of Structural Geology 10 (1), 3–8.

McFadzean, P.J., Dawers, N.H., Cowie, P.A., 1999. Field insights into prelinkage fault interaction. EOS, Transactions of the American Geophysical Union. 1999 Spring Meeting Supplement 80 (17), S331.

McGill, G.E., Stromquist, A.W., 1979. The Grabens of Canyonlands National Park, Utah: Geometry, mechanics, and kinematics. Journal of Geophysical Research 84 (B9), 4547–4563.

Moore, J.M., Schultz, R.A., 1999. Processes of faulting in jointed rocks of Canyonlands National Park, Utah. Geological Society of America Bulletin 111, 808–822.

Morley, C.K., Nelson, R.A., Patton, T.L., Munn, S.G., 1990. Transfer zones in the East African Rift System and their relevance to hydrocarbon exploration in rifts. American Association of Petroleum Geologists Bulletin 74, 1234–1253.

Morris, A.P., Ferrill, D.A., Henderson, D.B., 1996. Slip tendency analysis and fault reactivation. Geology 24, 275–278.

Peacock, D.C.P., Sanderson, D.J., 1991. Displacements, segment linkage, and relay ramps in normal fault zones. Journal of Structural Geology 13, 721–733.

Peacock, D.C.P., Sanderson, D.J., 1994. Geometry and development of relay ramps in normal fault systems. American Association of Petroleum Geologists Bulletin 78, 147–165.

Ramsay, J.G., Huber, M., 1987. The Techniques of Modern Structural Geology, Volume 2: Folds and Fractures. Academic Press, London.

Rowan, M.G., Jackson, M.P.A., Trudgill, B.D., 1999. Salt-related fault families and fault welds in the northern Gulf of Mexico. American Association of Petroleum Geologists Bulletin 83, 1454–1484.

Scholz, C.H., Dawers, N.H., Yu, J.Z., Anders, M.H., 1993. Fault growth and fault scaling laws: Preliminary results. Journal of Geophysical Research 98 (B12), 21951–21961.

Scott, R.B., 1990. Tectonic setting of Yucca Mountain, southwest Nevada. In: Wernicke, B.P. (Ed.). Basin and Range Extensional Tectonics Near the Latitude of Las Vegas, Nevada: Boulder, Colorado. Geological Society of America Memoir 176, pp. 251–282.

Simonds, W.F., Whitney, J.W., Fox, K., Ramelli, A., Yount, J.C., Carr, M.D., Menges, C.D., Dickerson, R., Scott, R.B., 1995. Map of fault activity of the Yucca Mountain area, Nye County, Nevada. U.S. Geological Survey Miscellaneous Investigations Series Map I–2520, scale 1:24,000.

Trudgill, B., Cartwright, J., 1994. Relay-ramp forms and normal-fault linkages, Canyonlands National Park, Utah. Geological Society of America Bulletin 106, 1143–1157.

U.S. Department of Energy, 1998. Viability assessment of a repository at Yucca Mountain, Volumes 1–5, DOE/RW-0508/V1-V5, December 1998.

U.S. Nuclear Regulatory Commission, 1999. Issue resolution status report, Key Technical Issue: Structural Deformation and Seismicity, Revision 2, September 1999.

Willemse, E.J.M., 1997. Segmented normal faults: Correspondence between three-dimensional mechanical models and field data. Journal of Geophysical Research 102, 675–692.

Willemse, E.J.M., Pollard, D.D., Aydin, A., 1996. Three-dimensional analyses of slip distributions on normal fault arrays with consequences for fault scaling. Journal of Structural Geology 18, 295–309.

Zoback, M.L., Anderson, R.E., Thompson, G.A., 1981. Cainozoic evolution of the state of stress and style of tectonism of the Basin and Range province of the western United States. Philosophical Transactions of the Royal Society of London A300, 407–434.